First-principles studies of phonon instabilities in AgI under high pressure

2008 J. Phys.: Condens. Matter 20 195218

(http://iopscience.iop.org/0953-8984/20/19/195218)

IOP PUBLISHING JOURNAL OF PHYSICS: CONDENSED MATTER

J. Phys.: Condens. Matter **20** (2008) 195218 (8pp) doi:10.1088/0953-8984/20/19/195218

First-principles studies of phonon instabilities in AgI under high pressure

Y Li[1], L J Zhang[1], T Cui[1], Y W Li[1], Y Wang[1], Y M Ma[1,2] and G T Zou[1]

[1] National Laboratory of Superhard Materials, Jilin University, Changchun 130012, People's Republic of China

[2] Laboratory of Crystallography, Department of Materials, ETH Zurich, HCI G 515, Wolfgang-Pauli-Strasse 10, CH-8093 Zurich, Switzerland

E-mail: mym@jlu.edu.cn (Y M Ma)

Received 30 November 2007, in final form 21 March 2008
Published 11 April 2008
Online at stacks.iop.org/JPhysCM/20/195218

Abstract

The dynamical instabilities of AgI are extensively studied using the density-functional perturbation theory to probe the mechanism of the pressure-induced phase transitions of wurtzite (WZ)/zinc-blende (ZB) → tetragonal → rocksalt (RS) → monoclinic → orthorhombic → CsCl. Analysis of the phonon calculations suggested that the pressure-induced instabilities of the transverse acoustic (TA) modes at the M/X points of zone boundaries for WZ/ZB AgI are responsible for the phase transitions of WZ/ZB → tetragonal. While the tetragonal → RS transition is not induced by phonon instability, but probably by energetic instability. Moreover, it is found that the transformation of the RS to monoclinic phase is driven by the softening of the TA mode at point X. The elastic constant calculations suggest that although the predicted elastic instabilities in WZ and ZB cannot independently induce the phase transition, they might couple with the softening phonon to lower the transition pressure. Pressure-induced metallization has been predicted for CsCl-type AgI from evidence of a significant band gap overlap. However, the CsCl phase of AgI is predicted to be dynamically unstable at the pressures under study.

1. Introduction

Silver iodide (AgI) has been extensively studied due to its fast ionic behavior within the α-phase (bcc structure), and also because it undergoes a number of phase transitions in a readily accessible temperature and pressure range [1]. The superionic conductor α-AgI, which is stable between 420 and 828 K at normal pressure, has been a subject of interest since it was discovered by Tubandt and Lorentz [2]. The iodine anions form a bcc lattice, and the silver cations exhibit superionic or fast-ion conduction by hopping between tetrahedral interstices. Conduction in α-AgI is high because Ag cations may move easily between these sites which, on average, are only 1/6th occupied [3].

At ambient conditions, AgI crystallizes in a mixed phase of wurtzite (WZ) and zinc-blende (ZB) with a ratio of 7:3 [4, 5], although the WZ phase is suggested to be more stable than the ZB phase from a thermodynamic point of view [6]. However, the energy difference between the WZ and ZB phases is so small that moderate grinding or compression could result in the formation of the ZB phase [7]. As a result, a sluggish phase transition from WZ to ZB occurs when a pressure of 0.1 GPa is applied [8]. With further compression, the ZB AgI is observed to undergo the transition to rocksalt (RS) structure through an intermediate tetragonal ($P4/nmm$) phase which exists in a narrow pressure range of 0.2–0.4 GPa [1] and the RS structure transforms to a monoclinic structure at 11.3 GPa [9].

Due to the limited investigations of the pressure-induced phase transitions at low temperature, the phase diagram for AgI below 200 K has not been fully understood up to now. Also, the ground state structure at the thermal limit for AgI has not yet been determined. Hanson *et al* [8] performed Raman scattering measurements at low temperature and high pressure and observed that AgI undergoes a phase transformation of WZ → RS at 76 K and 0.3 GPa. This transition sequence is obviously in contrast to that at ambient temperature [7]. Therefore the high pressure phase transition for WZ AgI depends strongly

on the temperature. Nevertheless, although there are no experimental reports on the structural transition of ZB AgI under pressure at low temperature, *ab initio* calculations [10] have suggested that at $T = 0$ K the ZB AgI will also take the phase transition sequence of ZB → tetragonal → RS as at room temperature [1]. It is clear that there exist abundant high pressure phase transformations with the formation of new polymorphs of AgI at low and high temperatures. To the best of our knowledge, the physically driven mechanism of the pressure-induced structural phase transitions in AgI remains unclear. Direct experimental evidence on the atomistic mechanisms of phase transition is still a big challenge. The dynamic instabilities are often responsible for phase transitions under pressure [11–19]. In particular, the predicted phonon softenings have been considered as the physically driven forces for the RS to CsCl phase transition in AgF and RS to monoclinic phase transitions in AgCl and AgBr through lattice dynamics and elastic instability studies [19]. Accordingly, it is expected that by systematically investigating the lattice dynamics behavior of AgI one can probe deeper into the nature of phase transitions under pressure. AgI is different from AgF/AgCl/AgBr in the ground state bonding nature and takes quite different phase transition sequences under pressure. Thus, with respect to our previous works [19] focusing only on the RS phase of AgF, AgCl, and AgBr, a full understanding of all possible high pressure phase transition sequences in AgI is proposed in this work. The systematic study of the pressure-induced phase transition for all possible high pressure phases in AgI will contribute significantly to a full understanding of the physically driven mechanism of the phase transition in all silver halides, which might serve as a prototype in probing the high pressure phase transition mechanism of other materials.

2. Method of calculation

The calculations have been carried out using a plane-wave pseudopotential scheme [20] within density-functional theory (DFT) [21, 22] as implemented in the Quantum-ESPRESSO package [23]. The Troullier and Marins [24] norm-conserving pseudopotentials were generated for Ag and I with valence configurations of $4d^{10}5s^1$ and $5s^25p^5$, respectively. The generalized gradient approximation (GGA) of the exchange–correlation functional is employed [25]. The electronic wavefunctions were expanded in a basis set of plane waves up to kinetic energy cutoffs of 120 Ryd for WZ, ZB, tetragonal, RS and monoclinic phases of AgI. Convergence tests gave the choices of a Monkhorst–Pack [26] **k**-point mesh of $8 \times 8 \times 8$ for RS and ZB AgI, $8 \times 8 \times 4$, $6 \times 6 \times 5$, $6 \times 8 \times 8$, $9 \times 9 \times 7$, $12 \times 12 \times 12$ for the WZ, tetragonal, monoclinic, orthorhombic, and CsCl phases of AgI, respectively. These choices allow the total energies to converge to ∼2 meV/atom. Linear response functions implemented in the Quantum-ESPRESSO package were calculated on $4 \times 4 \times 2$ and $4 \times 4 \times 3$ **q**-grids for WZ and tetragonal AgI, respectively, while a $4 \times 4 \times 4$ **q**-grid was used for both RS and ZB AgI. Interpolating the force constant calculated on these grids throughout the Brillouin zone (BZ) allows the calculation of the phonon frequencies at any given wavevector. Elastic constants were obtained from evaluations of the stress tensor generated by small strains, using the density-functional plane-wave technique as implemented in the CASTEP [27]. Note that the pseudopotentials used in CASTEP are also norm-conserving and identical in the electronic configurations and exchange–correlation functions to those used in the Quantum-ESPRESSO package.

Table 1. Calculated structural parameters of AgI in WZ, ZB, tetragonal, and RS structures. The experimental data from [9, 29], and [30] and the previously theoretical results from [28] are also listed for comparison.

		a (Å)	c (Å)	u	B_0 (MPa)	B_0'
WZ						
	This work	4.70	7.83	0.364	0.23	4.76
	Reference [28]	4.49	7.36	0.380	0.41	4.90
	Experiment	4.60[a]	7.52[a]	0.335[a]	0.24[b]	8.5[c]
ZB						
	This work	6.70			0.25	5.09
	Reference [28]	6.36			0.40	5.20
	Experiment	6.50[a]			0.24[b]	8.5[c]
Tetragonal						
	This work	4.62	6.83	0.268	0.06	5.95
RS						
	This work	6.20			0.32	5.50

[a] Reference [9].
[b] Reference [29].
[c] Reference [30].

3. Results

3.1. Structural properties

The equilibrium lattice parameters were determined by fitting the calculated total energy as a function of volume to the Murnaghan equation of state [28]. The calculated structural parameters for the ZB, WZ, tetragonal, and RS phase of AgI are listed in table 1 in comparison with the previous pseudopotential plane-wave theoretical calculation [29] within the local density approximation (LDA) and the experimental data [9, 30, 31]. It is found that the current theoretical lattice constants for ZB and WZ structures overestimate the experimental data by a maximum of 4.1%. This overestimation is typical from the implementation of GGA. However, one expects that the temperature effect might be another cause for this discrepancy. An excellent agreement in bulk modulus between theory and experiment is evidenced for these two phases. Note that the previous calculations within the LDA [29] underestimate the lattice constants by up to 2.5% as expected, but overestimate the bulk modulus up to 70.8%. The overall good agreement between theory and experiment in this study supports the choice of pseudopotentials and the GGA. From table 1, one also notices that the calculated B_0 for the WZ structure is very close to that in the ZB structure. This behavior is understandable due to the fact that these two structures have similar tetrahedral bonds up to the second neighbors, rendering the energy differences between them very small.

The Gibbs free energy $G = U + pV - TS$ as the appropriate thermodynamic potential governs the crystal stability for a given pressure and temperature. Here, as

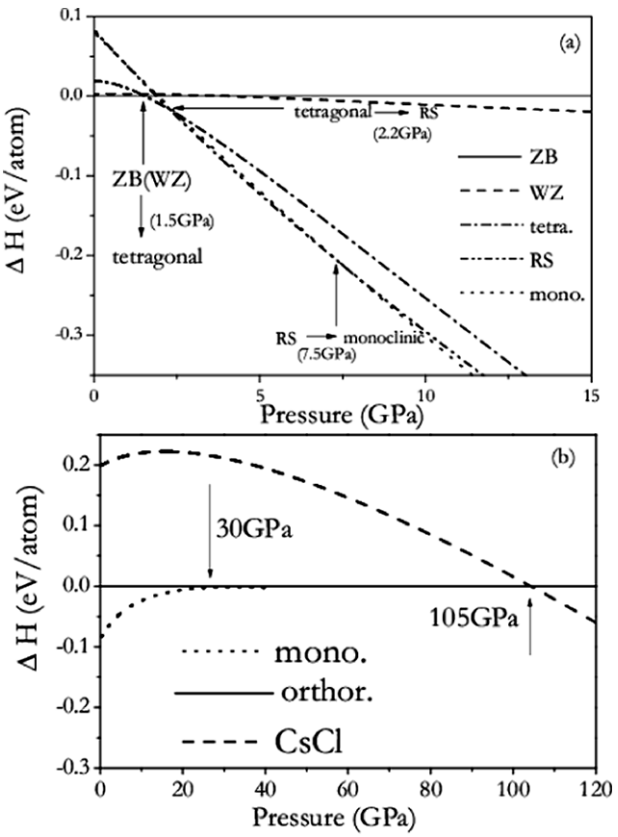

Figure 1. (a) Enthalpy difference H–H (ZB) versus pressure for WZ (short dashed line), tetragonal (dash dotted line), RS (dash dot dotted line), and monoclinic (dotted line) phases of AgI. (b) Enthalpy difference H–H (orthorhombic) versus pressure for monoclinic (dotted line) and CsCl phases of AgI.

a good approximation, we perform the calculations at zero temperature to simplify the Gibbs free energy as the enthalpy $H = E_{\text{tot}} + pV$. It is noteworthy that this simplification has previously been demonstrated to be very successful in producing correctly the free energy profiles at ambient temperatures. For a given pressure the crystallographic phase with the lowest enthalpy is the most stable one, and a crossing of two curves indicates a pressure-induced phase transition [10]. The enthalpy difference curves (relative to ZB structure) in WZ, tetragonal, RS, monoclinic, orthorhombic, and CsCl phases of AgI are plotted in figure 1, respectively. In figure 1(a), it is found that below 5 GPa, the enthalpy difference between WZ and ZB is very small (<2.3 meV) which is comparable to the calculation uncertainty of ∼2 meV/atom. This fact is mainly attributable to the similar tetrahedral bonding in WZ and ZB phases. Therefore, it is difficult to distinguish which phase is more stable at zero pressure and low temperature based on the current DFT. However, from the enthalpy calculation, it is clear that the phase transition sequence WZ/ZB → tetragonal → RS → monoclinic is expected when pressure is applied, as shown in figure 1(a). The transition pressures of WZ/ZB → tetragonal and tetragonal → RS are predicted to be ∼1.5 and 2.2 GPa, respectively. The current theory is in good agreement with a previous enthalpy calculation by Catti [10] who suggested that the phase transitions of ZB → tetragonal and tetragonal → RS occurred at 1.2 and 1.6 GPa, respectively. However, both theoretical predictions failed to produce the experimentally observed small transition pressures of 0.3 and 0.4 GPa, respectively, at room temperature. Neglecting the temperature effects in the calculations might be mainly responsible for this discrepancy. The fact that the intermediate tetragonal phase exists only in a very narrow pressure range of 1.5–2.2 GPa might preclude it from Raman observations, as suggested by [1]. This might be the cause for the failure in the observation of the tetragonal phase in the Raman measurement [8] at low temperature. Nevertheless, much experimental effort is needed to identify the existence of tetragonal phase during the WZ → RS transition.

At higher pressure, the phase transition of RS → monoclinic is calculated to occur at 7.5 GPa which is in acceptable agreement with the experimental value of 11.3 GPa. However, up to now, no experimental measurements were performed above 15 GPa [9]. In the cases of AgCl and AgBr, the phase transitions of RS → CsCl through the intermediate monoclinic and orthorhombic phases were determined experimentally [9, 32] and theoretically [33]. Therefore, the subsequent phase transition at higher pressure for AgI may also adopt the sequence of monoclinic → orthorhombic → CsCl [34]. The enthalpy curves (relative to orthorhombic phase) for monoclinic and CsCl structures are plotted in figure 1(b). The transition pressure of monoclinic → orthorhombic is calculated to be 32 GPa, which is consistent with the previous theoretical result of 30 GPa [34]. It is important to note that the CsCl phase takes over the stability at pressures of above 105 GPa (figure 1(c)).

3.2. Dynamical properties under pressure

3.2.1. WZ phase. Figure 2 shows our *ab initio* phonon dispersion curves and the projected phonon density of states (DOS) at different volumes for WZ AgI with the experimental neutron inelastic scattering data [35] at zero pressure and 160 K. Twelve vibrational modes are shown as expected since there are four atoms in the primitive unit cell. An interesting feature is that only four phonon modes are observed at the $\boldsymbol{A}$ symmetry point due to the existence of two doubly degenerate longitudinal modes and two fourfold-degenerate transverse modes. At the $\boldsymbol{K}$ point, there is a noticeable splitting between the lowest transverse optical (TO) mode and the longitudinal acoustic (LA) mode, while they are degenerate along the directions of $\boldsymbol{A}$–$\boldsymbol{H}$ (**S**), $\boldsymbol{H}$–$\boldsymbol{L}$ (**S**′), and $\boldsymbol{L}$–$\boldsymbol{A}$ (**R**). One also observes six phonon branches along the high symmetry directions of **S**, **S**′, and **R**. Along the least symmetric directions of **T** and $\sum$, the 12 phonon branches fully split. It is noteworthy that the theoretical phonon dispersion is in good agreement with that in a shell-model calculation [31]. The experimental phonon dispersion data (symbols) are reproduced with reasonably good accuracy by the present calculation except for the optical phonons which are systematically underestimated by up to 18%. The calculated equilibrium lattice constants a (4.70 Å) and c (7.83 Å) are larger than the experimental values of 4.60 and 7.52 Å, respectively. A

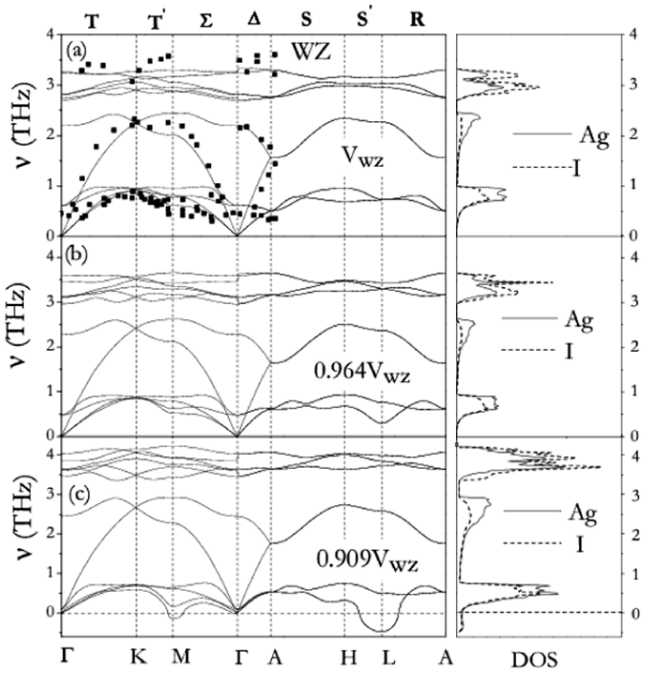

Figure 2. The calculated phonon frequencies (solid lines) and projected phonon DOS of WZ AgI at different volumes (V_{WZ} is the equilibrium volume of the WZ AgI), along with the experimental phonon dispersion data (symbols) at $T = 160$ K and ambient pressure from [35].

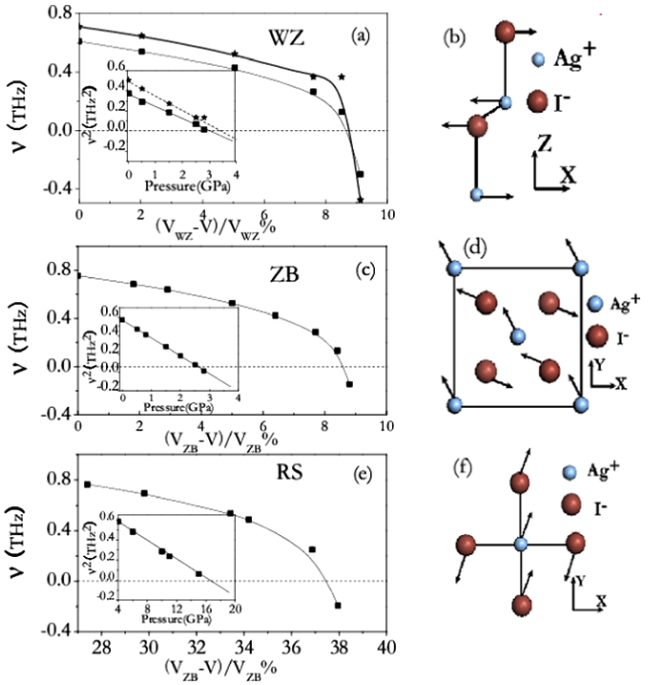

Figure 3. The main figure of (a) shows the calculated phonon frequencies of TA($\boldsymbol{M}$) (squares) and TA($\boldsymbol{L}$) (stars) in WZ AgI as a function of volume. The lines through the calculated data points represent the fitted curves using a B-spline. Inset: the calculated squared phonon frequency ν^2 as a function of pressure for TA($\boldsymbol{M}$) (squares) and TA($\boldsymbol{L}$) (stars), respectively. The solid line through the data points is a linear fit. (b) The eigenvectors for TA($\boldsymbol{M}$) in WZ AgI and the arrows representing the displacements of the Ag cations and I anions in the primitive cell. The main figures of (c) and (e) show the calculated frequencies of TA($\boldsymbol{X}$) as a function of volume for ZB and RS AgI, respectively. The insets in (c) and (e) show the ν^2 as a function of pressure, respectively. (d) and (f) are the eigenvectors for TA($\boldsymbol{X}$) and the arrows represent the displacements of the Ag cations and I anions in the ZB and RS structures, respectively.

(This figure is in colour only in the electronic version)

decrease in lattice constant is expected to efficiently enhance the phonon frequency, especially for optical phonons. This fact is mainly responsible for the large discrepancy between the calculations and experiments. The flat dispersions of the optical modes in the high frequency region of 2.8–3.3 THz and the transverse optical and acoustic modes in the low frequency region of 0.6–1.0 THz give rise to the two sharp maxima in the projected phonon DOS (right panel of figure 1(a)). Because the atomic mass of Ag (107.9) is comparable to that of I (126.9), the Ag (dashed line) and I (solid line) atomic vibrations are fully coupled to each other.

From figures 2(b) and (c), it is evident that upon volume decrease most of the optical modes experience an upward shift while the lowest TO modes and the transverse acoustic (TA) phonon modes move to lower frequency, indicating a negative Grüneisen parameter, $\gamma_j(q) = -\partial \ln \upsilon_j(q)/\partial \ln V$ for mode j, where q is the wavevector, υ is the frequency, and V is the volume. At a volume of $0.909V_{WZ}$ (V_{WZ} is the equilibrium volume of the WZ AgI), there appear unstable modes with dominant instabilities at $\boldsymbol{M}$ and $\boldsymbol{L}$ points, signaling a structural instability in the WZ phase. Imaginary frequencies, plotted as negative, are obtained from negative eigenvalues of the dynamical matrix. Figure 3(a) shows the variations of the frequencies of the TA ($\boldsymbol{M}$) and TA ($\boldsymbol{L}$) modes with volume for WZ AgI. Both modes are predicted to show a softening behavior with decreasing volume. However, accurate phonon frequency determination suggests that the TA ($\boldsymbol{M}$) mode softens to zero first. The WZ phase would become unstable at a critical pressure P_c at which the frequency of the TA ($\boldsymbol{M}$) mode becomes zero. In an attempt to estimate P_c, the pressure dependence of the TA ($\boldsymbol{M}$) mode frequency was fitted by a phenomenological function [36] of $\upsilon^2 = (\upsilon_0^2 - aP)$, as shown in the inset of figure 3(a). As a result, P_c' giving $\upsilon = 0$ is estimated to be 3.0 GPa ($V = 0.917V_{WZ}$) for WZ AgI. Since the transition between WZ and tetragonal phases is of first order, the phase transition is suggested to occur below P_c as P_c is the upper limit [36]. Therefore, the difference between the predicted transition pressure of ∼3.0 GPa by phonon instability and ∼1.5 GPa by enthalpy curves (figure 1) is acceptable. Consequently, the physically driven force for this transition is suggested to be attributable to the TA ($\boldsymbol{M}$) phonon instability. The schematic representation of atomic vibrations for the TA ($\boldsymbol{M}$) mode is shown in figure 3(b). It is suggested that the anti-paralleled displacements of the Ag cation and I anion along the direction of the **X** axis (**X** represents the $\boldsymbol{a}$ axis and Y represents the $\boldsymbol{c}$ axis) with pressure induces the instability of WZ AgI and results in the formation of tetragonal AgI.

3.2.2. ZB phase. Although the phonon dispersion curves of WZ AgI at zero pressure have been measured using the inelastic neutron scattering technique, there are no

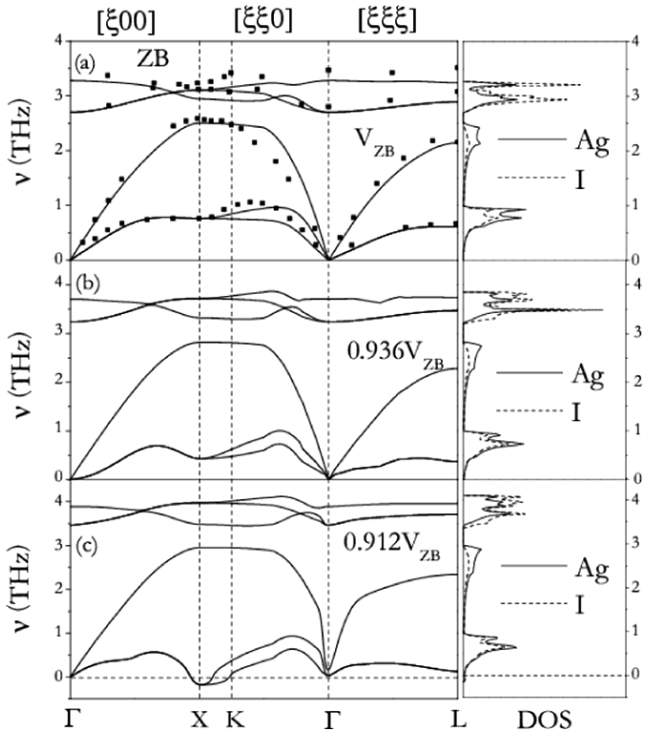

Figure 4. Calculated phonon frequencies (solid lines) and the projected phonon DOS in ZB AgI at different volumes (V_{ZB} is the equilibrium volume of the ZB AgI), together with the experimental phonon dispersion data (symbols) for ZB CuBr at ambient conditions, scaled by Ma^2_{AgI}/Ma^2_{CuBr} [34].

experimental measurements of the phonon dispersions in the ZB phase [35]. ZB AgI possesses similar properties to ZB CuBr due to the fact that it has similar ionicity of $f = 0.73$. Therefore, the experimental data for the phonon dispersions of ZB CuBr, scaled by the homology criterion of interatomic forces $\nu_{AgI}/\nu_{CuBr} = (Ma^2_{CuBr}/Ma^2_{AgI})^{1/2}$, where ν, M, and a represent the phonon frequency, atomic mass, and lattice constant, respectively, can be used as a benchmark for the validity of the current theoretical model [35]. Figure 4 shows the calculated phonon dispersion curves and the projected phonon DOS of ZB AgI at different volumes along with the corrected experimental data for ZB CuBr at ambient pressure [36]. It is significant that the agreement between theory and experiment is found to be strikingly good at zero pressure. Note that the current *ab initio* phonon calculations agree better with experiments than those in the valence-shell mode calculations [35], especially for the acoustic phonon branches. This fact is understandable due to the methodological accuracy within the linear response DFT.

In ionic crystals, long range macroscopic electric fields arise which are associated with long wave longitudinal optical phonons. These electric fields are a result of the long range character of the Coulomb interaction, and are responsible for the well-known phenomenon of LO–TO splitting [38], that is, the shift in frequency between longitudinal optical and transverse optical phonons at the BZ center. The origin of this splitting can be understood if one considers that the LO mode can create an extra restoring force due to the electric field between the anions and cations. In general, the amplitude of the splitting can be characterized by the Born effective charges tensor and dielectric tensor. Note that because of the symmetry of the ZB AgI, the Born effective charge tensors and dielectric tensor are all isotropic. Furthermore, the sum of the Born effective charges over the ions in a unit cell must be zero (so $Z_{Ag} = -Z_I$). The formula about the splitting of LO–TO for binary compounds with cubic phase is written as $\omega^2_{LO} - \omega^2_{TO} = 4\pi Z^2/\mu\Omega\varepsilon$ [39], where ω_{L0} and ω_{T0} represent the longitudinal and transverse frequencies, μ the reduced mass, Ω the volume of the unit cell, and ε the dielectric constants. Therefore, calculating Born effective charges can account for the splitting of LO–TO. At zero pressure, $Z_{Ag} = 1.34e$ and $\varepsilon = 5.26$ give a value of 0.58 THz for the splitting of LO–TO which is in good agreement with the experimental value of 0.67 THz [35, 37].

With decreasing volume, the TO, LO, and LA phonon modes of ZB AgI shift to higher frequency, while the TA mode decreases. At a volume of $0.912V_{ZB}$ (V_{ZB} is the equilibrium volume of the ZB AgI) the TA phonons at the $\boldsymbol{X}$ point have softened to imaginary frequencies, signaling a structural instability. Figure 3(c) shows the variation of the frequency of the TA ($\boldsymbol{X}$) mode with volume for ZB AgI. The squared phonon frequencies ν^2 for the TA branch at the $\boldsymbol{X}$ point with pressure are plotted in the inset of the figure 3(c). The critical pressure P_c corresponding to zero TA ($\boldsymbol{X}$) phonon frequency is predicted to be 2.9 GPa ($V = 0.914V_{ZB}$) [1]. Since the phase transition of ZB $\rightarrow$ tetragonal is also of first order, it is understandable that the estimated P_c is larger than 1.6 GPa ($V = 0.947V_{ZB}$) in the enthalpy calculation (figure 1) [10]. The schematic representation of eigenvectors for the TA phonon mode at the X point is shown in figure 3(d). The arrows represent the directions of the atomic vibrations for the Ag cations and the I anions, respectively. Inspection of the phonon eigenvectors shows that this mode involves alternate shuffles of (001) planes. The displacements of the Ag and I atoms form 104.5° and 14.5° with respect to the direction of the X axis (X axis along [100] and Y axis along [010]), respectively. The atomic movements along the directions of the eigenvectors in the (001) planes are, thus, closely related to the phase transition from ZB to tetragonal.

3.2.3. Tetragonal phase. The lattice dynamics and the projected phonon DOS for the tetragonal AgI with volume are presented in figure 5. The strong coupling between Ag and I atomic vibrations is also evidenced due to the similar atomic masses of Ag and I, as indicated in the projected phonon DOS. It should be pointed out that upon volume decreasing ($0.765V_{ZB}$, where V_{ZB} is the equilibrium volume of the ZB AgI) the entire phonon branches move to higher frequency (figure 5(b)), suggesting dynamical stability for the tetragonal AgI under pressure. Therefore, the observed phase transition of tetragonal to RS is not related to the soft phonon; instead, it is more likely to be energetically induced as shown from the enthalpy calculation.

3.2.4. Rocksalt phase. The theoretical phonon dispersion curves and the projected phonon DOS for RS AgI at different volumes are shown in figure 6. It can be clearly seen that at

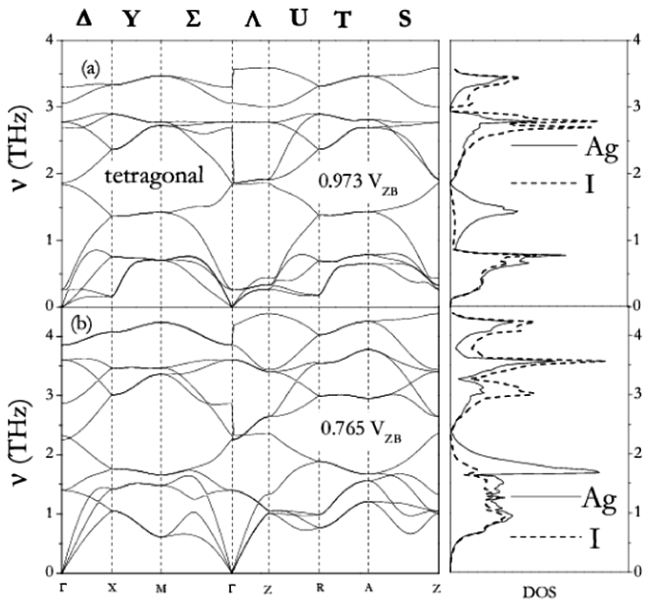

Figure 5. Calculated phonon dispersion curves and projected phonon DOS for tetragonal AgI at different volumes.

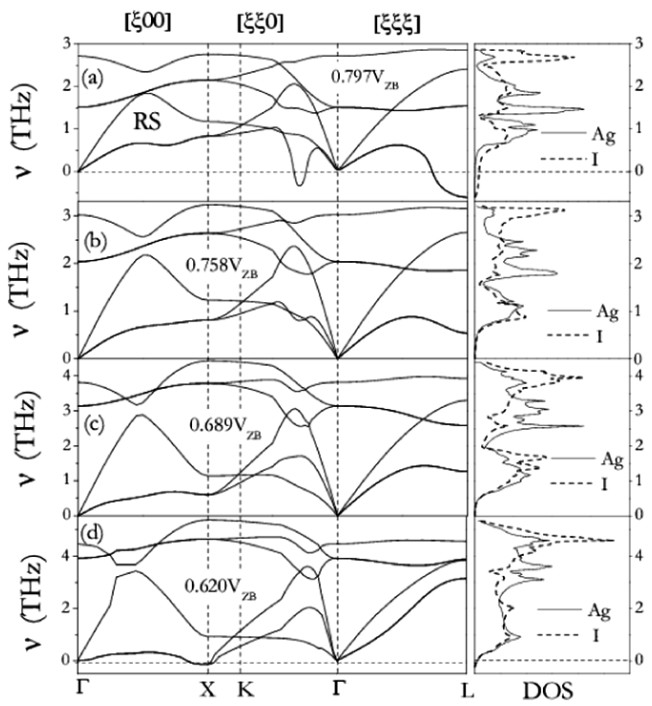

Figure 6. Calculated phonon dispersion curves and projected phonon DOS of RS AgI at different volumes.

zero pressure (figure 6(a)) there are imaginary frequencies at the $\boldsymbol{L}$ (0.5 0.5 0.5) and $\boldsymbol{q}$ (0.45 0.45 0) points. However, with increasing pressure, at ∼2 GPa ($V = 0.758V_{ZB}$) (figure 6(b)), all the phonons become stable. This behavior indicates that high pressure is a favorable condition for the formation of RS structure, in agreement with experimental observations. It was predicted that the most imaginary TA ($\boldsymbol{L}$) modes become positive at 1.1 GPa ($V = 0.772V_{ZB}$). Since the RS AgI has a lower enthalpy than that in the tetragonal structure at 1.6 GPa ($V = 0.753V_{ZB}$), the RS AgI is, thus, dynamically and thermodynamically stable at this pressure. As shown in figures 6(c) and (d), with decreasing volume, the TO, LO, and LA phonon modes shift to higher frequency, while the TA mode decreases. At a volume of $0.620V_{ZB}$ the TA ($\boldsymbol{X}$) mode becomes imaginary, indicating a structural instability. The variation of the frequency of the TA ($\boldsymbol{X}$) mode with volume is shown in the main figure of figure 3(e). The calculated transition pressure is 15.8 GPa ($V = 0.629V_{ZB}$) from the inset of figure 3(e). This transition pressure is somewhat larger than the experimental observation of 11.3 GPa and the theoretical value of ∼7.5 GPa from the enthalpy calculation at the RS → monoclinic transition (figure 1(a)). Inspection of the atomic displacements for the TA ($\boldsymbol{X}$) mode shown in figure 3(f) suggests that the Ag cation and I anion are displaced in the opposite directions and the displacement of the Ag cation forms an angle of 66.1° with respect to the direction of the X axis (X axis along [100] and Y axis along [010]).

3.3. Elastic constants

The elastic properties define the behavior of a material that undergoes stress, deforms, and then recovers and returns to its original shape after stress ceases. Thus, the elastic behavior plays an important role in understanding the structural stability. The strain we used is 0.003. Table 2 compares the calculated elastic constants with the experimental results [40] at zero pressure for WZ AgI. The present results show a good agreement with the measurements for C_{11}, C_{33}, and C_{44} while there are discrepancies of no more than 18% for C_{12} and C_{13}. These discrepancies may be induced by the effect of temperature since the measurements of C_{12} and C_{13} were performed at 298 K, while the experimental data of C_{11}, C_{33}, and C_{44} were obtained at 20 K. It is well known that the criteria for the elastic stability for a WZ structure is that $C_{11} + C_{12}$, $C_{11} + C_{12} - 4C_{13} + 2C_{33}$, C_{33}, $(C_{11} - C_{12})/4$, and C_{44} are all positive. From figure 7(a), one can conclude that the WZ phase is still elastically stable at 3 GPa ($V = 0.917V_{WZ}$) at which point the WZ AgI becomes dynamically unstable.

Table 2. Calculated elastic constants of C_{11}, C_{33}, C_{44}, C_{12}, and C_{13} with units of MPa for WZ AgI, together with the experimental results from [40] at ambient pressure.

	C_{11}	C_{33}	C_{44}	C_{12}	C_{13}
This work	3.32	3.90	0.43	2.55	2.32
Experiment	3.74	4.39	0.41	2.13	1.96

The experimental determination of the elastic constants requires single crystals, which normally are cut, polished, and oriented at room temperature before measurements [34]. Therefore, the lack of experimental data for ZB AgI is probably due to the experimental difficulties. The generally accepted elastic stability criteria for a cubic crystal is that C_{44} and $C_s = (C_{11} - C_{12})/2$ are all positive [41]. The variation of the calculated elastic constants with pressure for ZB and RS AgI is shown in figures 7(b) and (c), respectively. For ZB phase (figure 7(b)), it is found that C_{11} and C_{12} show linearly increasing trends with pressure, while C_{44} and C_s soften. For

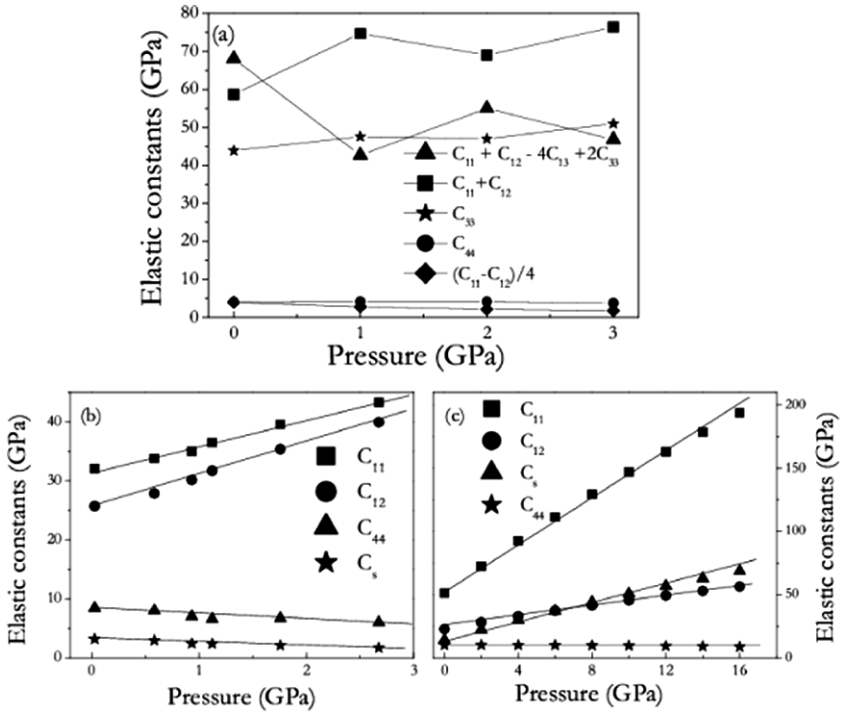

Figure 7. Variations of the elastic constants (solid symbols) for WZ (a), ZB (b), and RS (c) AgI with pressure. The solid lines are linear fits to the calculated results.

RS AgI (figure 7(c)), C_{44} shows similar softening behavior as that for ZB AgI, but C_s increases with pressure. It is noteworthy that although C_{44} and C_s in ZB AgI and C_{44} in RS AgI soften with pressure, they still remain positive under a certain pressure at which the phonons soften to zero frequency. Therefore, we conclude that the pressure-induced structural phase transitions for WZ, ZB, and RS AgI have no direct relation to the elastic instabilities which are related to the long-wavelength part of the transverse branch near the center of the first BZ. The phase transitions in these three phases are mainly dominated by the phonon instability. It should be pointed out that the phonon softening might be coupled with the elastic instabilities of C_{44} (C_s) and then be efficiently lower than the transition pressures corresponding to zero phonon frequency as in the case of the soft-mode driven phase transitions of Rutile-type structures [42, 43]. These couplings might improve the transition pressure predicted by the soft mode getting closer to the experimental observation.

3.4. Pressure-induced metallization

The pressure-induced insulator–metal transition is of particular interest. It has been proposed [44] that AgCl and AgBr become metallic under high pressure with the formation of the CsCl phase. Therefore it is interesting to explore the possibility of metallization of AgI within the CsCl phase through band structure calculations. Since the CsCl AgI is predicted to be stable only beyond 105 GPa (figure 1(c)), calculations of band structure and electronic DOS for CsCl AgI are, thus, performed at 105 GPa, as presented in figure 8. The metallization is clearly predicted by evidence of a significant band overlap at the M and X points (figure 8(a)).

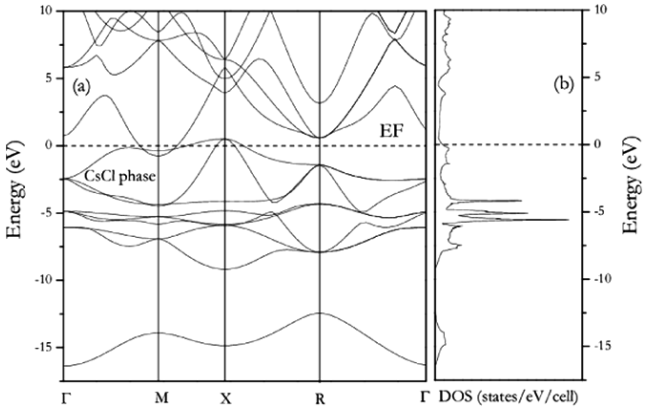

Figure 8. Electronic band structure and density of states for CsCl AgI at 105 GPa.

To check the dynamical stability of the CsCl AgI, we plot out its full phonon dispersion at 105 GPa in figure 9. Interestingly, large imaginary phonon modes near points X and M are predicted, indicating a dynamical instability of this phase. The existence of imaginary phonons in CsCl AgI might preclude its formation at high pressure in spite of it being energetically favorable beyond 105 GPa. However, the current phonon calculation is based on the harmonic model and the effect of anharmonicity might become very important at high temperature. As a result, the anharmonicity could help to stabilize the CsCl phase of AgI at finite temperature. Further experiments, therefore, are expected to verify the existence of the CsCl phase in AgI.

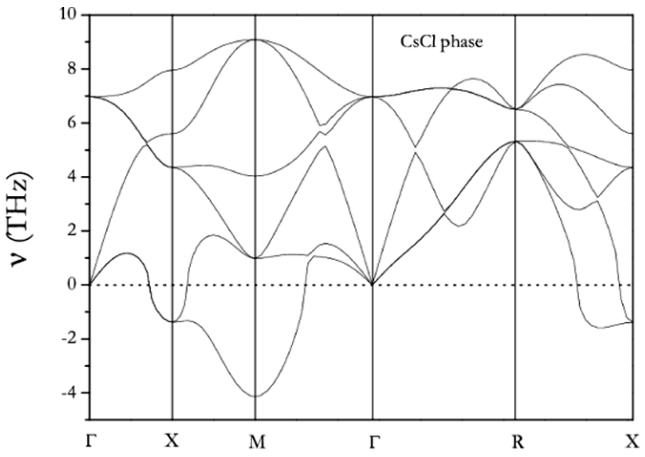

Figure 9. Calculated phonon dispersion curves for CsCl AgI at 105 GPa.

4. Conclusion

A complete phase transition sequence of WZ/ZB → tetragonal → RS → monoclinic → orthorhombic → CsCl for AgI is fully explored by the total energy, lattice dynamics, and elastic constant calculations within the density-functional theory. The lattice dynamics instabilities of WZ, ZB, and RS AgI were clearly revealed to be responsible for the pressure-induced phase transitions of WZ → tetragonal, ZB → tetragonal, and RS → monoclinic, respectively. While the tetragonal → RS transformation is not induced by phonon instability, it is likely to be caused by energetic instability. The elastic constant calculations suggest that although the predicted elastic instabilities in WZ and ZB cannot independently induce the phase transition, they might couple with the softening phonon to lower the transition pressure. Furthermore, a metallic phase of AgI is proposed, though it is dynamically unstable.

Acknowledgments

We are grateful for financial support from NSAF of China (No. 10676011), the China 973 Program (No. 2005CB724400), the NBRPP of China (No. 2001CB711201), the NDFCEM (No. 20050183062), the SRF for ROCS, SEM, the Program for 2005 New Century Excellent Talents in University, and the 2006 Project for Scientific and Technical Development of Jilin Province.

References

[1] Keen D A and Hull S 1993 *J. Phys.: Condens. Matter* **5** 23
[2] Tubandt C and Lorentz E 1914 *Z. Phys. Chem.* **87** 58
Tubandt C and Lorentz E 1914 *Z. Phys. Chem.* **87** 543
[3] Nield V M and Hayes W 1995 *Defect Diffus. Forum* **125/126** 37
[4] Maskasky Joe E 1991 *Phys. Rev.* B **43** 5769
[5] Berry C R 1967 *Phys. Rev.* **161** 848
[6] Burley G 1964 *J. Phys. Chem.* **68** 1111
[7] Maskasky Joe E 1991 *Phys. Rev.* B **43** 5769
[8] Hanson R C, Fjeldly T A and Hochheimer D 1975 *Phys. Status Solidi* b **70** 567
[9] Hull S and Keen D A 1999 *Phys. Rev.* B **59** 750
[10] Catti M 2005 *Phys. Rev.* B **72** 064105
[11] Nardelli M B, Baroni S and Giannozzi P 1995 *Phys. Rev.* B **51** 8060
[12] Clatterbuck D M, Krenn C R, Cohen M L and Morris J W Jr 2003 *Phys. Rev. Lett.* **91** 135501
[13] Persson K, Ekman M and Ozolinš V 2000 *Phys. Rev.* B **61** 11221
[14] Baroni S, Gironcoli S de, Corso A and Gianozzi P 2001 *Rev. Mod. Phys.* **73** 515
[15] Ozolinš V and Zunger A 1999 *Phys. Rev. Lett.* **82** 767
[16] Kim K, Ozolins V and Zunger A 1999 *Phys. Rev.* B **60** R8449
[17] Ma Y, Tse J S and Klug D D 2003 *Phys. Rev.* B **67** 140301(R)
[18] Ma Y, Tse J S and Klug D D 2004 *Phys. Rev.* B **69** 064102
[19] Li Y, Zhang L, Cui T, Ma Y, Zou G and Klug D D 2006 *Phys. Rev.* B **74** 054102
Li Y, Zhang L, Cui T, Li Y, Ma Y, He Z and Zou G 2007 *J. Phys.: Condens. Matter* **19** 425217
[20] Pick R M, Cohen M H and Martin R M 1970 *Phys. Rev.* B **1** 910
[21] Hohenberg P and Kohn W 1964 *Phys. Rev.* **86** B864
[22] Kohn W and Sham L J 1965 *Phys. Rev.* **140** A1133
[23] Baroni S, Corso A Dal, Gironcoli S de, Giannozzi P, Cavazzoni C, Ballabio G, Scandolo S, Chiarotti G, Focher P, Pasquarello A, Laasonen K, Trave A, Car R, Marzari N and Kokalj A http://www.pwscf.org/
[24] Troullier N and Martins J L 1991 *Phys. Rev.* B **43** 1993
[25] Perdew J P and Burke K 1996 *Int. J. Quantum Chem.* **S 57** 309
Perdew J P, Burke K and Ernzerhof M 1996 *Phys. Rev. Lett.* **77** 3865
[26] Monkhorst H J and Pack J D 1976 *Phys. Rev.* B **8** 5188
[27] Segall M, Lindan P, Probert M, Pickard C, Hasnip P, Clark S and Payne M 2002 *J. Phys.: Condens. Matter* **14** 2717
[28] Mumaghan F D 1994 *Proc. Natl Acad. Sci. USA* **50** 697
[29] Nunes G S, Allen P B and Martins J L 1998 *Phys. Rev.* B **57** 5098
[30] Hanson R C, Fjeldly T A and Hochheimer H D 1975 *Phys. Status Solidi* a **70** 567
[31] Vaidya S N and Kennedy G C 1971 *J. Phys. Chem. Solids* **32** 951
[32] Kusaba K, Syono Y, Kikegawa T and Shimomura O J 1995 *J. Phys. Chem. Solids* **56** 751
[33] Catti M and Piazza L Di 2006 *J. Phys. Chem.* B **110** 1576
[34] Catti M 2006 *Phys. Rev.* B **74** 174105
[35] Bührer W, Nicklow R M and Brüesch P 1978 *Phys. Rev.* B **17** 3362
[36] Samara G A and Peercy P S 1981 *Solid State Physics* vol 36 , ed H Ehrenreich, F Seitz and D Turbnbull (New York: Academic)
[37] Hoshino S, Fujii Y, Harada J and Axe J S 1976 *J. Phys. Soc. Japan* **41** 965
[38] Ashcroft N W and Mermin N D 1976 *Solid State Physics* (Philadelphia: HRM International Editions) p 548
[39] Liu J and Vhra Y K 1994 *Phys. Rev. Lett.* **72** 4105
[40] Fjeldly T A and Hanson R C 1974 *Phys. Rev.* B **10** 3569
[41] Wang J, Yip S, Phillpot S R and Wolf D 1993 *Phys. Rev. Lett.* **71** 4182
[42] Lodziana Z, Parlinski K and Hafner J 2006 *Phys. Rev.* B **63** 134106
[43] Hellwig H, Goncharov A F, Gregoryanz E, Mao H and Hemley R J 2003 *Phys. Rev.* B **67** 174110
[44] Louis C N, Iyakutti K and Malarvizhi P 2004 *J. Phys.: Condens. Matter* **16** 1577